MSc in Photonics

PHOTONICS**BCN**

Universitat Politècnica de Catalunya (UPC)
Universitat Autònoma de Barcelona (UAB)
Universitat de Barcelona (UB)
Institut de Ciències Fotòniques (ICFO)

http://www.photonicsbcn.eu

Master in Photonics

MASTER THESIS WORK

Photoconductive antennas for terahertz radiation

Sergio Revuelta Martínez

Supervised by Dr. Romeu Robert, Jordi, (UPC)
and Dr. Santos Blanco, Maria Concepción, (UPC)

Presented on date 19th July 2018

Registered at

Escola Tècnica Superior
d'Enginyeria de Telecomunicació de Barcelona

Photoconductive antennas for terahertz radiation

Sergio Revuelta Martínez[1]

[1] Dept. of Signal Theory & Commun., Polytech. Univ. Catalonia, Barcelona, Spain

E-mail: sergio.revuelta@alu-etsetb.upc.edu

Abstract. A model to simulate the dynamics of the electrons/holes pairs when they are generated in a semiconductor material by the application of an optical field and accelerated by a bias electrostatic field is presented. This model helps in the estimation of the photocurrent induced by the mobility of carriers to get a prediction of the THz power provided by a set of different prototypes of photoconductive antennas that have been designed and discussed.

Keywords: Photoconductive antennas, THz radiation, Photoconductor

1. Introduction

There is a region in the electromagnetic spectrum within 3000 and 30 μm of wavelength known as the THz gap between the microwave band (100 GHz) and the far infra-red band (10 THz). This gap often called the last frontier for being the last portion of the spectrum to be covered by convenient sources and detectors [1] has increased the interest of many scientist and engineers over the last two decades for its wide potential applications [2] such as: Spectroscopy [3] since vibration resonances of molecules and solids are in the THz regime; Imaging [4,5] due to a higher penetration depth and to the water sensitivity, THz waves can be used in security or tomography applications and see though objects that are opaque in the visible or in the IR region; Communications [6], THz region offers the potential for wireless systems with much higher bandwidth than the systems used nowadays. While WIFI systems have a maximum speed of up to 400 Mbits/s, in 2016 it was demonstrated a transmission of 20 Gbits/s at 300 GHz [7].

In order to generate THz waves different ways have been proposed to obtain such radiation. Terahertz Quantum Cascade (THz-QC) techniques can deliver the maximum amount of radiative power, up to 145 mW at 4.1 THz and 0.65 mW at 1.59 THz in continuous wave mode (cw) [8], but at cryogenic temperatures, 160 K and 71 K respectively. Another possibility is the generation of THz waves with non-linear optics by means of optical rectification in non-linear (NL) crystal. However the efficiency of the NL crystals is very low and there is a need of perfect phase-matching to exploit all the volume of the crystal while the THz absorption by phonons limits the bandwidth. The generation of 1 mW of THz average power needs a laser with a power of 10 W [9].

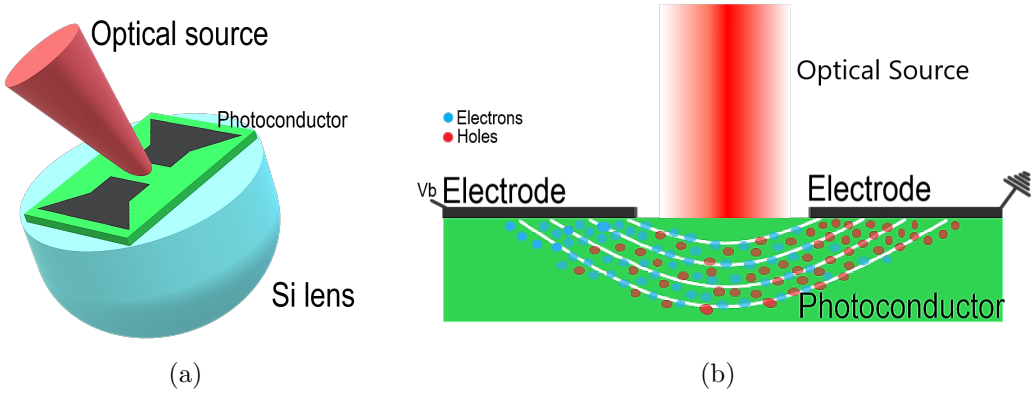

(a) (b)

Figure 1. Schematic diagram and operation concept of photoconductive antenna. (a) Photoconductor connected to a bowtie THz antenna. (b) Cross section illustration of photocarrier generation at the antenna gap showing the flux lines of the electric field in white lines.

The most suitable method to obtain such desired radiation is with photoconductive antennas (PCA), where basically achieving a current that changes on picoseconds time scales it is possible to obtain a THz wave [1, 10].

PCA are based in the optoelectronic phenomena, where a laser and a voltage applied through some electrodes can induce a current by the generation of electrons/holes pairs in a semiconductor with the appropriate energy gap. This concept is illustrated in Figure 1.

Most of the investigations have been in the study of the PCA with lasers operating in the time domain (TD), whose pulses have a duration in the order of the sub-picoseconds [1] generating broad band THz radiation. With PCA-TD it has been demonstrated a radiation power up to 3.8 mW over a frequency range from 0.1 THz to 5 THz at an optical power of the laser of 240 mW [11].

Even when PCA-TD are very useful in a wide range of applications such as spectroscopy or security, for communications it is needed narrow band radiation instead of broad band. An interesting way of generating THz radiation in cw is the photomixing in photoconductors, often called photoconductive mixing using lasers working in cw mode (frequency domain, FD).

2. Theoretical model

The approach we have studied in this work is similar to three-wave mixing, but instead of considering NL optics, optoelectronics. Two continuous lasers with an offset in their frequency can generate a photocurrent at the difference of frequency [10]. This photocurrent eventually generate a THz radiation with the appropriate load such as an antenna.

The most general solution for the current (eq. 1) is retrieved from the expressions of the photocarrier generation rate obtained from the Fermi's golden rule, and from

the optoelectronic impulse response which is derived from the Ramo-Shockley theorem [10, 12]. This solution is often called the Brown model.

$$I_{ph} = e\mathbb{R}\left\{\int_{V_{tot}}\left(g_0(G_e+G_h) + G_e\frac{\tilde{g}e^{i\Delta\omega t}}{1-i\Delta\omega\tau_e} + G_h\frac{\tilde{g}e^{i\Delta\omega t}}{1-i\Delta\omega\tau_h}\right)dV\right\} \quad (1)$$

$$g_0 = \frac{\alpha}{Z_0 h\nu}\left(E_{opt,1}^2 + E_{opt,2}^2\right) \qquad \& \qquad \tilde{g} = \frac{2\alpha}{Z_0 h\nu}\left(E_{opt,1}^2 \cdot E_{opt,2}^2\right)e^{-i\phi} \quad (2)$$

Where $\Delta\omega$ is the frequency offset between the lasers, V_{tot} is the integration volume and $G_{e,h}$ are the gains ($\frac{\tau_{e,h}}{T_{e,h}}$), that are calculated with the lifetime of the electrons/holes ($\tau_{e,h}$) and with the transit time ($T_{e,h}$, it is the time that an electron or a hole should spend in their trip from the point where it is generated to the electrode though the electric field lines). The transit time has a dependence with the bias applied, as the velocity of the carriers grows almost linearly with the electric field until the saturation velocity is reached [13].

Eq. 2 shows the photocarrier generation rate in a phasor form ($g_0 + \mathbb{R}\{\tilde{g}e^{i\Delta\omega t}\}$), there h is the Planck constant, ν is the frequency of the lasers, Z_0 is the intrinsic impedance of the dielectric, that can be solved with the electrical permittivity and the magnetic permeability ($Z_0 = \sqrt{\frac{\mu}{\epsilon}}$) [14], the coefficients α, e, ϕ refers to the absorption coefficient of the dielectric at the working wavelength, the electron charge and the phase difference between the two lasers and $E_{opt,1}$ and $E_{opt,2}$ are the optical electric field in the medium at the point where absorption occurs.

Although this model provides an interesting description of the photocurrent generated in a PCA-FD, it does not take into account the saturation of the photocurrent that occurs in the photoconductor due to the screening effect, which is, without considering the thermal heating, the limiting factor of the PCA [17]. The screening effect is due to the generation of an electric field that counteracts the applied DC field reducing the acceleration of the electrons/holes pairs and hence the radiative output power [18–21].

The step to simulate the screening effect with two continuous waves is non-obvious and no studies have been published about it due to photomixing. The movement of charges give rise to a charge distribution which generates an electrostatic field in the opposite direction than the applied across the electrodes. Therefore the final electric field inside the photoconductor will be the electric field induced by the voltage applied minus the electric field generated by the distribution of charges. That will lead us to a non-linear equation for the current. In order to perform a first approximation, we have considered the electric field changes due to the induced current (eq. 3), whose change implicates a variation in the electric field as well. Solving the non-linear equations system for different optical powers that involve the electric field and the current (eq. 1), we can obtain the variation of current as function of the optical power.

$$E = E_B - \frac{I}{\sigma S} \quad (3)$$

Where E_B is the bias electric field, I is the current, σ is the conductivity and S is the integration surface.

3. Equivalent circuit

An equivalent circuit is a powerful tool that helps for quantifying and maximizing the efficiency on an electronic device. The performance of a PCA is affected by different phenomena as the geometry of the PCA, the interaction of the laser with the substrate or the radiation properties of the antenna. To considerer all these features a Thévenin equivalent circuit is proposed.

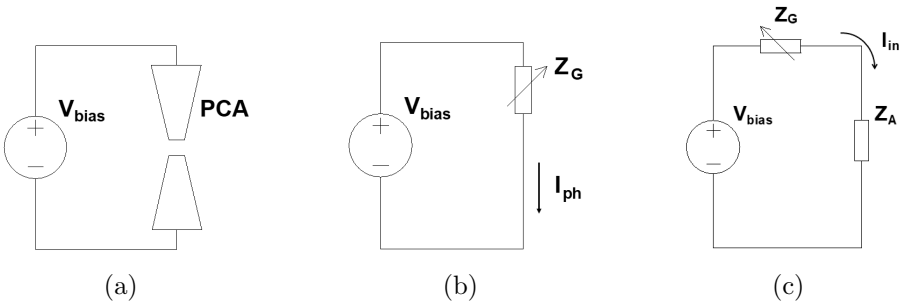

Figure 2. (a) PCA schematic representation. (b) Equivalent circuit of photocurrent process. (c) Equivalent circuit of transmitting antenna.

Figure 2. shows the equivalent circuit proposed. The antenna is represented by a load impedance $Z_A = R_A + i\chi_A$. We represent the generator with a variable resistance, that is because the lasers will generate a current that will depend on their optical power, however we can considerer in a descriptive way that the lasers are generating a variable impedance ($Z_G = \frac{V}{I_{ph}}$). The current at antenna input terminals will be $I_{in} = \frac{V}{Z_G + Z_a}$, that allows us to determine the total power produced (P_{tot}) and the power delivered to the antenna (P_A), which will be the power radiate by the antenna without considering ohmic losses.

$$P_{tot} = \frac{1}{2}\mathbb{R}\left\{V I_{in}^{*}\right\} = \frac{1}{2}\frac{|V|^2 (Z_G + R_A)}{|Z_G + Z_A|^2} \tag{4}$$

$$P_A = \frac{1}{2}|I_{in}|^2 R_A = \frac{1}{2}\frac{|V|^2 R_A}{|Z_G + Z_A|^2} \tag{5}$$

4. Simulations

We have studied different geometries of PCA for THz emission, representative examples presented in this work are: H-dipole (PCA1), Bow-tie (PCA2), Log-spiral (PCA3) and Sierpinski 4^{th} order (PCA4) (Figure 3.)

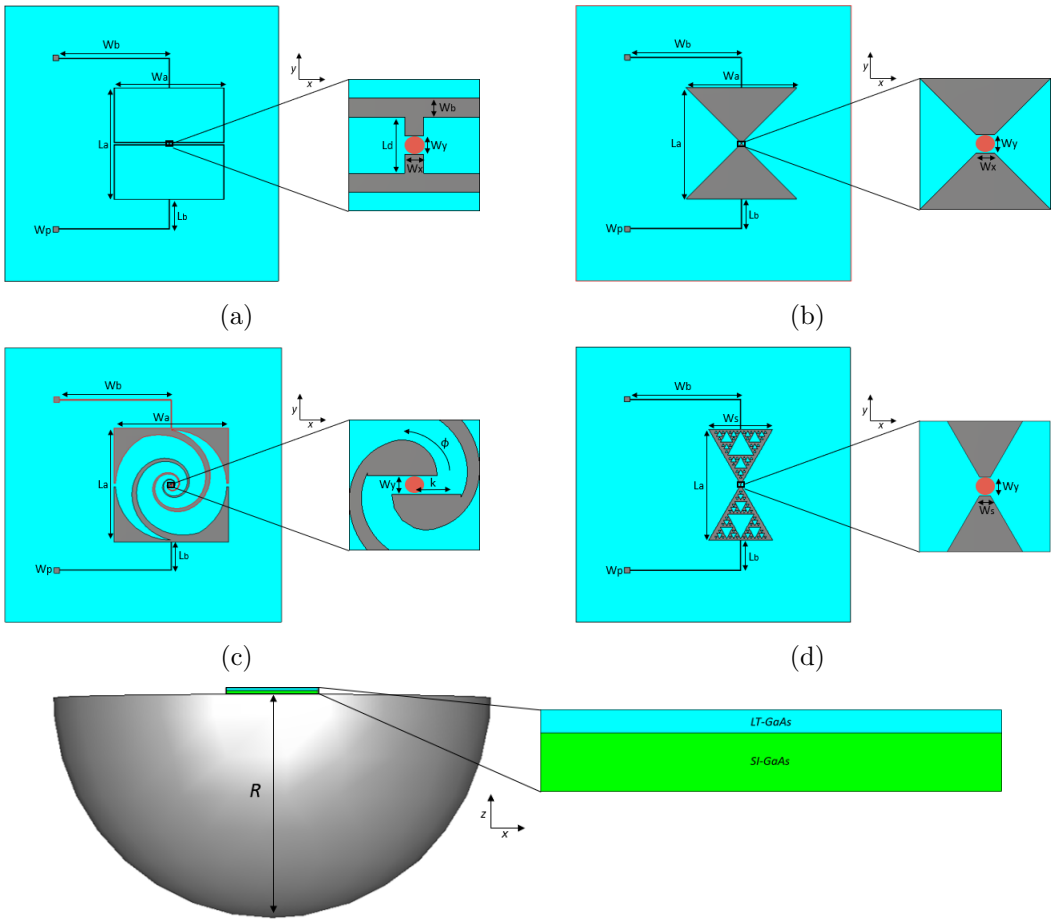

Figure 3. PCA geometries studied. The blue colour represents the LT-GaAs substrate, green represents the SI-GaAs substrate on which the LT-GaAs will be grown, grey represents the metallization of the antenna. (a) H-dipole: gap size $W_x = W_y = 10$ μm, metallization width $W_b = 10$ μm and dipole length $L_d = 30$ μm. (b) Bow-tie: gap size $W_x = W_y = 10$ μm and slope=± 1. (c) Log-spiral: $r_1 = ke^{\alpha\phi}$, $r_2 = ke^{\alpha(\phi-\delta)}$, initial radius $k = 23$ μm, $\alpha = 0.2401$, opening angle $\delta = 30$, $\phi = [0 : 2\pi N]$, number of turns $N = 2.6$ and length gap $W_y = 10$ μm. (d) Sierpinski: Fractal antenna 4^{th} order, gap size $W_s = 5.77$ μm and $W_y = 10$ μm. The overall sizes of the antenna are $L_a = W_a = 2000$ μm, $W_s = 1154.7$ μm, $W_b = 2000$ μm and $L_b = 545$ μm. Bias pad width $W_p = 100$ μm. In the zoomed-in view, it is show the laser distribution in red colour, $D_{laser} = 10$ μm. (e) Lateral view of a PCA. The radius of the Si lens is $R = 12$ mm and the heights of the LT-GaAs and SI-GaAs are 2 μm and 525 μm respectively.

4.1. Photocurrent

We have developed a simulation model to understand the dynamics of the electrons/holes pairs in the LT-GaAs substrate when a voltage is applied across the electrodes and thus be able to calculate the gains of the photogeneration process. The results presented here correspond to the same bias voltage applied for all the different geometries (40 V). Firstly, it has been calculated the electrons/holes trajectories when two continuous lasers with a central frequency of 800 nm and an offset of 2.5 nm generates the carriers

and the bias voltage applied drift them to the electrodes.

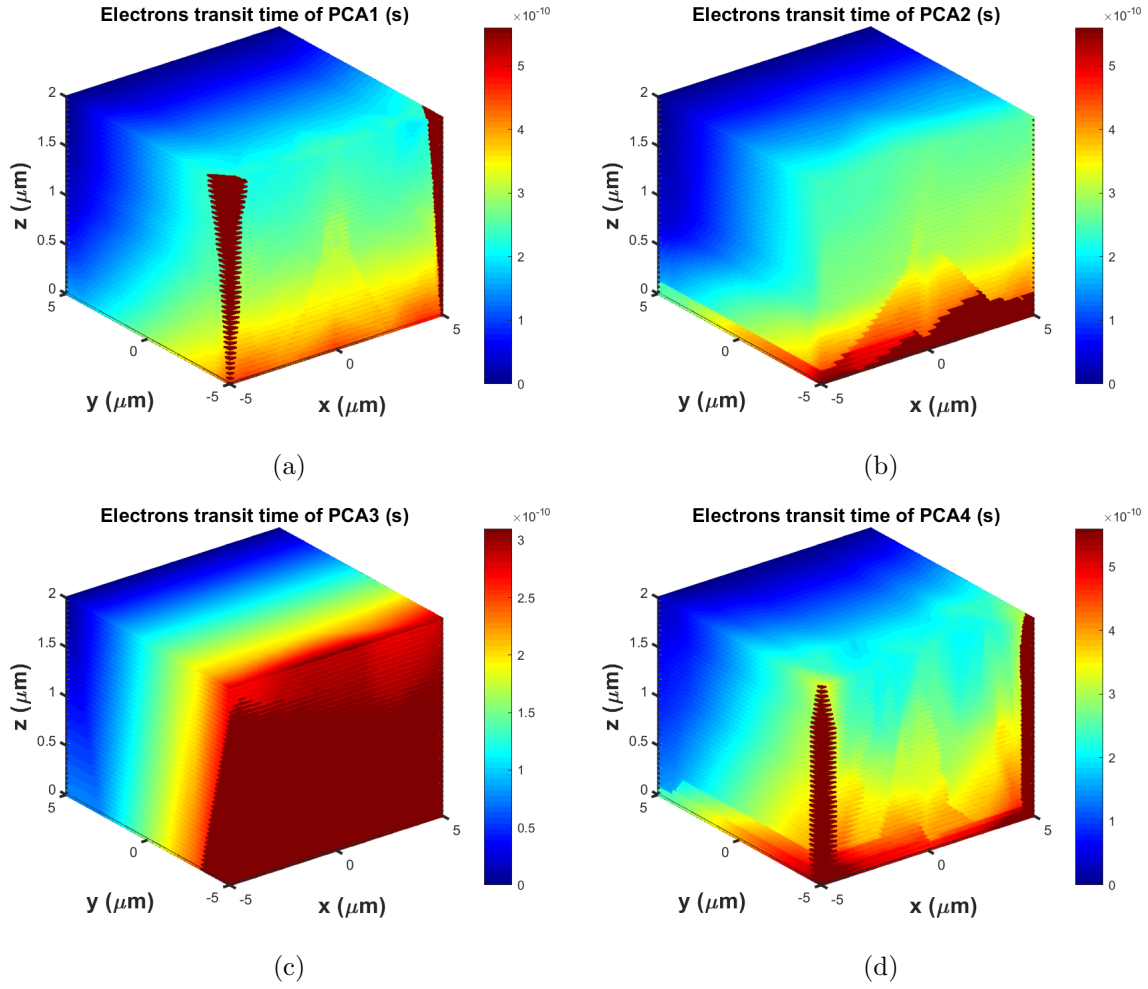

Figure 4. Simulated electrons transit time in the region of LT-GaAs where the carriers photogeneration will occurs. Electrodes are placed in Y=5 μm and Y=-5 μm positions. (a) PCA1. (b) PCA2. (c) PCA3. (d) PCA4.

Figure 4. and Figure 5. show the transit times of the photogenerated electrons/holes pairs. There, is represented the transit time of the electrons for the entire volume and the transit time for holes and electrons in the plane YZ-X=0.

The simulation is an iterative model that solves the trajectory of the carriers depending on the local field in differential regions of a mesh that correspond with the LT-GaAs substrate, this field was obtained by means of electrostatic simulations applying a potential difference in the pads of the PCA. Once it has been generated a carrier in a certain point of the mesh, it will have 26 different possibilities of movement as we have 3 degrees of freedom that correspond with the electric field in the three dimensions. By evaluating the electric field in that position can be estimated what will be the new position to which the carrier will move. Knowing the points of the mesh on which the carrier has been in his trip from the point on it has been generated to the electrode we can estimate the length travelled by the carrier. The transit time can be

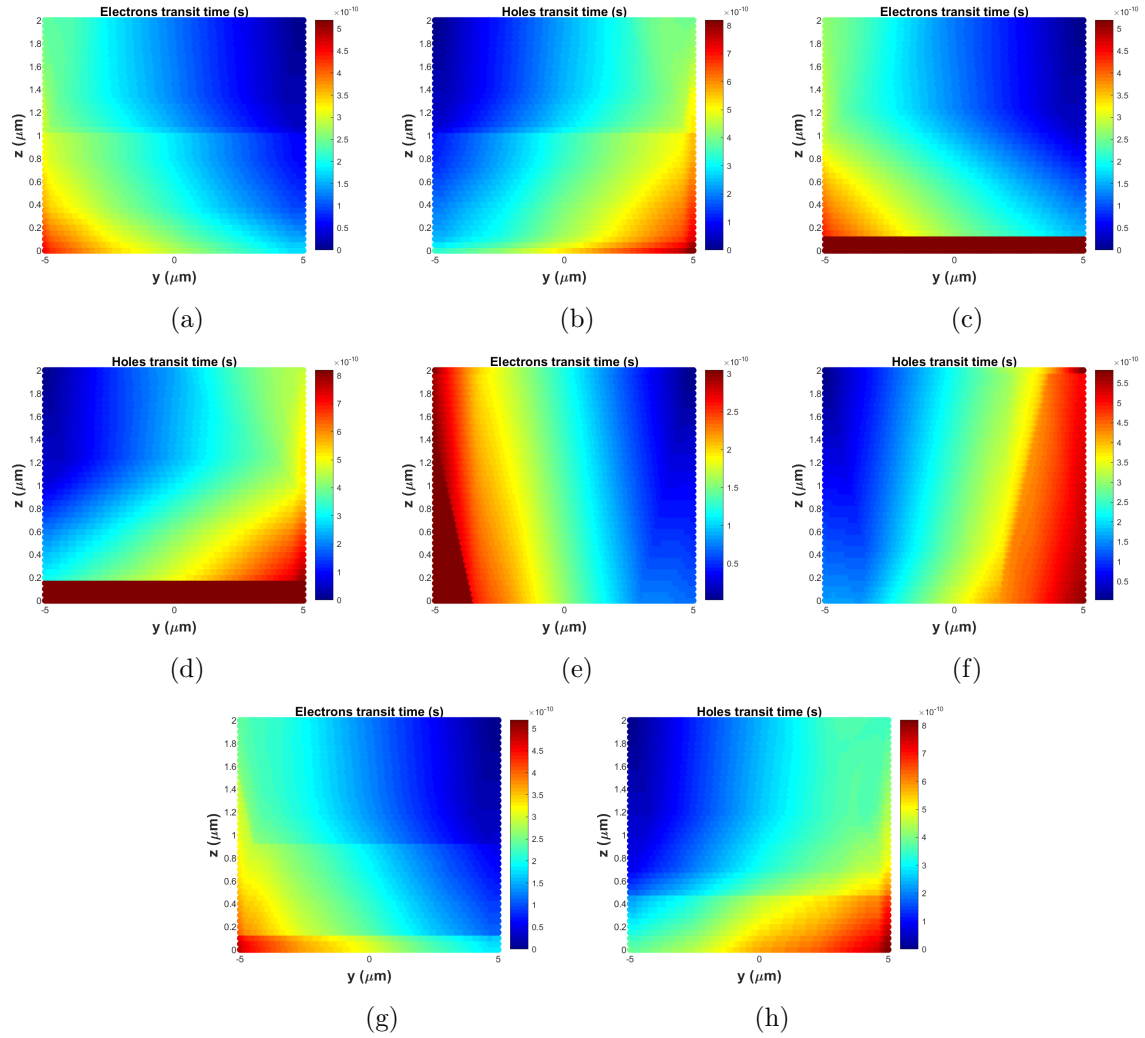

Figure 5. Simulated electrons transit time in the region of LT-GaAs where the carriers photogeneration will occurs in plane X=0. Electrodes are placed in Y=5 μm and Y=-5 μm positions. (a) and (b) Electrons and holes transit times of PCA1. (c) and (d) Electrons and holes transit times of PCA2. (e) and (f) Electrons and holes transit times of PCA3. (g) and (h) Electrons and holes transit times of PCA4.

calculated with the length travelled and the average velocity of the trip.

Once it has been calculated the initial photoconductive gains with the trajectories and velocity of the carriers, optical simulations were done due to obtain the optical electric fields inside the LT-GaAs substrate. Then we can solve the photocurrent generated by the two lasers solving the NL system composed by the eq. (1) and (3) as function of the optical power.

Figure 6. shows the estimated photocurrent in the PCAs. In our work we do not find that, a change in the polarization of any laser in the optical simulations will induce a variation in the photocurrent. All geometries studied are able to generate almost the same photocurrent and it makes sense as all the designs have the same substrate and almost the same gap dimensions. Log-spiral antenna is the one which is able to deliver

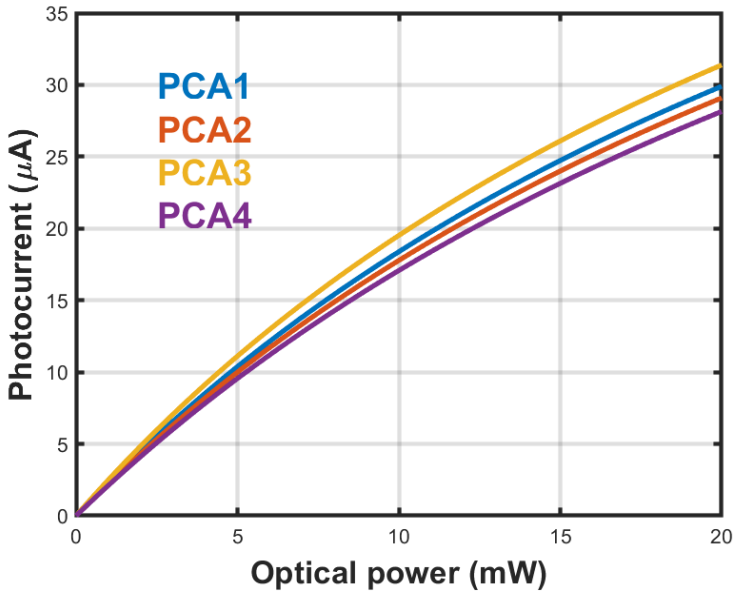

Figure 6. Simulated photocurrent from the different PCAs studied.

the maximum amount of photocurrent, that it is coherent comparing the transit times for the different PCAs.

4.2. Radiative output power

The radiative output power of the antenna will depend on its impedance. Different simulations have been done to solve the radiation patterns and be able to obtain the resonances of each antenna. A higher photocurrent generated in the PCA will lead us to a higher radiative output power, however, that does not mean the PCA with higher current generated will have the maximum output power as that also depends on the antenna impedance. To calculate the output power of the PCAs the equation for the power delivered to the antenna (eq. 5) has been used.

The simulations of the radiation patterns of the antennas have been done for a frequency range from 0.275 to 0.725 THz. This range has been chosen targeting the three frequency windows for communications in 0.325, 0.485 and 0.675 THz [6]. Figure 7. shows the estimated output power as function of the frequency for the 4 different PCAs studied. Each PCA has a characteristic radiation pattern which is translated into a different output power as function of the frequency, that correspond with the intrinsic resonances of the PCA.

Bow-tie and Sierpinski antennas are seem to have a broadband behaviour while H-dipole and Log-spiral have resonances in characteristic frequencies. The most interesting case is without any doubt the spiral geometry as it has a high resonance in a certain frequency (0.475 THz), very near to the window of 0.485 THz.

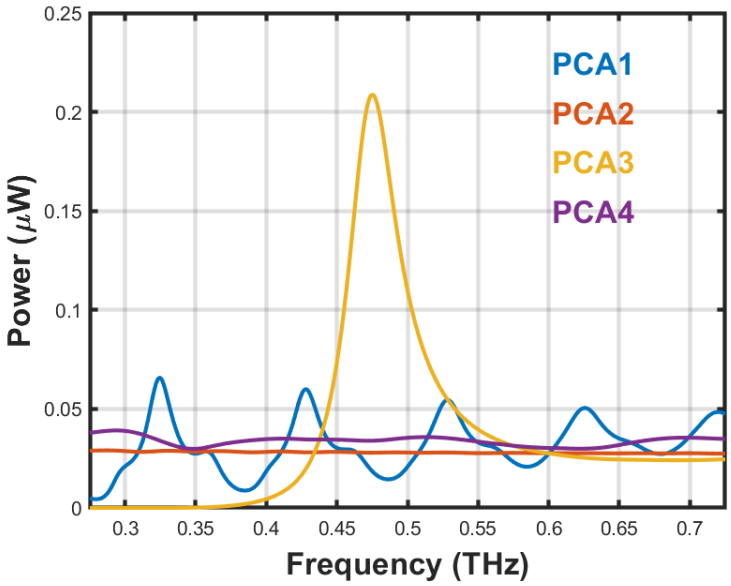

Figure 7. Simulated output power for a frequency radiation range that goes from 0.275 to 0.725 THz with an optical power of 20 mW for the different PCAs studied.

5. Conclusions

A model to simulate the dynamics of the electrons/holes pairs in a substrate once they are generated by the application of two lasers with an offset in their frequency has been developed, the application of a bias voltage across some electrodes drift the carriers inducing a separation of charges that has been taken into account to considerer the screening effect in the induced photocurrent. We have seen clearly how the photocurrent does not grow linearly with the optical power.

It has been designed different geometries of photoconductive antennas for THz radiation. The study of the geometries presented here allow us the estimation of the photocurrent generated in the antennas and their radiation patterns that depends on the characteristic resonances of each antenna. We have calculated the theoretical output power of the antenna approximating the designs with a Thévening circuit and considering no ohmic losses in the process. The difference between the 4 types of antennas presented in their photogenerated current, dynamics of the electrons/holes inside the substrate and the radiative patterns have been shown in full view. Based in our results the dimensions of the PCA prototypes to be manufactured have been established.

The geometry used will be very sensitive to the application pretended either narrowband or broadband radiation. This study will be helpful in future investigations of systems for narrowband or broadband emission in THz based on photomixing.

CST studio®, a commercial software, was used to simulate the electrostatic, optical field and the radiation patterns of the antennas. The simulations of the electrons/holes trajectories and calculations of the photocurrent and radiative output power were

programmed in MATLAB®.

References

[1] Burford N M and El-Shenawee M O 2017 *Optical Engineering* **56** 010901–1–20
[2] Redo-Sanchez A and Zhang X C 2008 *IEEE Quantum Electron.* **14** 260–269
[3] Hangyo M, Tani M and Nagashima T 2005 *International Journal of Infrared and Millimeter Waves* **26** 1661–1690
[4] Llombart N, Dengler R J and Cooper K B 2010 *IEEE Antennas and Propagation Magazine* **52** 251–259
[5] Doyle R, Lyons B, Lettington A, McEnroe T, Walshe J, McNaboe J and Curtin P 2005 *Proceedings of SPIE* **5789** 101–108
[6] Shams H and Seeds A 2017 *Optics&Photonics* **28**
[7] Song H J, Kosugi T, Hamada H, Tajima T, Moutaouakil A E, Matsuzaki H, Kawano Y, Takahashi T, Nakasha Y, Hara N, Fujii K, Watanabe I, Kasamatsu A and Yaita M 2016 *2016 IEEE MTT-S International Microwave Symposium (IMS)* 1–4
[8] Kumar S and Lee A W 2008 *IEEE Quantum Electron.* **14** 333–344
[9] Hebling J, Yeh K L, Hoffmann M C and Nelson K A 2008 *IEEE Quantum Electron.* **14** 345–353
[10] Brown E R 2003 *International Journal of High Speed Electronics and Systems* **13** 497–545
[11] Yardimci N T, Yang S H, Berry C W and Jarrahi M 2015 *IEEE Transactions on Terahertz Science and Technology* **5** 223–229
[12] Shockley W 1938 *Journal of Applied Physics* **9** 635–636
[13] Sze S M and Kwok K N 2007 *Physics of semiconductor devices* vol 6.3 (John Wiley & Sons)
[14] Cheng D K 2013 *Field and Wave Electromagnetics* 2nd ed (Pearson Higher Ed USA)
[15] Dan Y, Zhao X and Mesli A 2015 *ArXiv e-prints*
[16] Achuthan M K and Bhat K N 2007 *Fundamentals of Semiconductos Devices* (Tata McGraw-Hill)
[17] Saeedkia D 2011 Terahertz photoconductive antennas: Principles and applications *Proceedings of the 5th European Conference on Antennas and Propagation (EUCAP)* pp 3326–3328
[18] Kim J H, Polley A and Ralph S E 2005 *Opt. Lett.* **30** 2490–2492
[19] Moon K, Lee I M, Shin J H, Lee E S, Kim N, Lee W H, Ko H, Han S P and Park K H 2015 *Scientific Reports* **5** 13817
[20] Berry C W, Wang N, Hashemi M R, Unlu M and Jarrahi M 2013 *Nature Communications* **4** 1622
[21] Loata G C, Thomson M D, Loffler T and Roskos H G 2007 *Appl. Phys. Lett.* **91** 232506